



Supplement of

Estimated regional CO₂ flux and uncertainty based on an ensemble of atmospheric CO₂ inversions

Naveen Chandra et al.

Correspondence to: Naveen Chandra (naveennegi@jamstec.go.jp) and Prabir K. Patra (prabir@jamstec.go.jp)

The copyright of individual parts of the supplement might differ from the article licence.

Table S1. A comprehensive list of CO₂ observations from 50 sites for optimizing fluxes, taken from GML/NOAA - Global Monitoring Laboratory/National Oceanic and Atmospheric Administration (38 sites), CSIRO - Commonwealth Scientific and Industrial Research Organisation (4 sites), LSCE/IPSL - Laboratoire des sciences du climat et de l'environnement/Institut Pierre Simon Laplace (1 site), SIO-CO2 – Scripps Institution of Oceanography (2 sites), SAWS – South African Weather Services (1 site), ECCC- Environment and Climate Change Canada (1 site), and JMA – Japan Meteorological Agency (3 sites). Data until 2019 are taken from obspack_co2_1_GLOBALVIEWplus_v6.1_2021-03-01, and JMA data are taken from WDCGG. Extension to GVplus_6.1 for 2020 is compiled from GML/NOAA data and WDCGG as appropriate.

| Site_Name | Lat | Long | Alt(m) | Operating Institute |
|---------------------------------------|-------|--------|--------|---------------------|
| co2_alt_surface-flask_1Representative | 82.5 | -62.5 | 190.0 | GML/NOAA |
| co2_asc_surface-flask_1Representative | -8.0 | -14.4 | 85.0 | GML/NOAA |
| co2_ask_surface-flask_1Representative | 23.3 | 5.6 | 2710.0 | GML/NOAA |
| co2_azr_surface-flask_1Representative | 38.8 | -27.4 | 19.0 | GML/NOAA |
| co2_bmw_surface-flask_1Representative | 32.3 | -64.9 | 30.0 | GML/NOAA |
| co2_brw_surface-flask_1Representative | 71.3 | -156.6 | 11.0 | GML/NOAA |
| co2_cba_surface-flask_1Representative | 55.2 | -162.7 | 21.3 | GML/NOAA |
| co2_cgo_surface-flask_1Representative | -40.7 | 144.7 | 94.0 | GML/NOAA |
| co2_chr_surface-flask_1Representative | 1.7 | -157.2 | 0.0 | GML/NOAA |
| co2_crz_surface-flask_1Representative | -46.4 | 51.8 | 197.0 | GML/NOAA |
| co2_eic_surface-flask_1Representative | -27.2 | -109.4 | 47.0 | GML/NOAA |
| co2_gmi_surface-flask_1Representative | 13.4 | 144.7 | 0.0 | GML/NOAA |
| co2_hba_surface-flask_1Representative | -75.6 | -26.2 | 30.0 | GML/NOAA |
| co2_hun_surface-flask_1Representative | 47.0 | 16.7 | 248.0 | GML/NOAA |
| co2_ice_surface-flask_1Representative | 63.4 | -20.3 | 118.0 | GML/NOAA |
| co2_izo_surface-flask_1Representative | 28.3 | -16.5 | 2372.9 | GML/NOAA |
| co2_key_surface-flask_1Representative | 25.7 | -80.2 | 1.0 | GML/NOAA |
| co2_kum_surface-flask_1Representative | 19.5 | -154.8 | 3.0 | GML/NOAA |
| co2_mhd_surface-flask_1Representative | 53.3 | -9.9 | 5.0 | GML/NOAA |

| | | | | |
|---|-------|--------|--------|-----------|
| co2_mid_surface-flask_1Representative | 28.2 | -177.4 | 11.0 | GML/NOAA |
| co2_mlo_surface-flask_1Representative | 19.5 | -155.6 | 3397.0 | GML/NOAA |
| co2_nmb_surface-flask_1Representative | -23.6 | 15.0 | 456.0 | GML/NOAA |
| co2_nwr_surface-flask_1Representative | 40.1 | -105.6 | 3523.0 | GML/NOAA |
| co2_psa_surface-flask_1Representative | -64.9 | -64.0 | 10.0 | GML/NOAA |
| co2_rpb_surface-flask_1Representative | 13.2 | -59.4 | 15.0 | GML/NOAA |
| co2_sey_surface-flask_1Representative | -4.7 | 55.5 | 2.0 | GML/NOAA |
| co2_shm_surface-flask_1Representative | 52.7 | 174.1 | 23.0 | GML/NOAA |
| co2_smo_surface-flask_1Representative | -14.2 | -170.6 | 42.0 | GML/NOAA |
| co2_spo_surface-flask_1Representative | -89.0 | -24.8 | 2810.0 | GML/NOAA |
| co2_sum_surface-flask_1Representative | 72.6 | -38.4 | 3209.5 | GML/NOAA |
| co2_syo_surface-flask_1Representative | -69.0 | 39.6 | 14.0 | GML/NOAA |
| co2_tap_surface-flask_1Representative | 36.7 | 126.1 | 16.0 | GML/NOAA |
| co2_ush_surface-flask_1Representative | -54.8 | -68.3 | 12.0 | GML/NOAA |
| co2_uta_surface-flask_1Representative | 39.9 | -113.7 | 1327.0 | GML/NOAA |
| co2_uum_surface-flask_1Representative | 44.5 | 111.1 | 1007.0 | GML/NOAA |
| co2_wis_surface-flask_1Representative | 30.0 | 35.1 | 151.0 | GML/NOAA |
| co2_wlg_surface-flask_1Representative | 36.3 | 100.9 | 3810.0 | GML/NOAA |
| co2_zep_surface-flask_1Representative | 78.9 | 11.9 | 474.0 | GML/NOAA |
| co2_cfa_surface-flask_2Representative | -19.3 | 147.1 | 2.0 | CSIRO |
| co2_mqa_surface-flask_2Representative | -54.5 | 159.0 | 6.0 | CSIRO |
| co2_cya_surface-flask_2Representative | -66.3 | 110.5 | 47.0 | CSIRO |
| co2_maa_surface-flask_2Representative | -67.6 | 62.9 | 32.0 | CSIRO |
| co2_ams_surface-insitu_11Representative | -37.8 | 77.5 | 55.0 | LSCE/IPSL |
| co2_bhd_surface-flask_426Representative | -41.4 | 174.9 | 85.0 | SIO-CO2 |
| co2_rk1_surface-flask_426Representative | -29.2 | -177.9 | 2.0 | SIO-CO2 |
| co2_cpt_surface-insitu_36_marine | -34.4 | 18.5 | 230.0 | SAWS |

| | | | | |
|---|------|-------|-------|------|
| co2_fsd_surface-insitu_6_allvalid | 49.9 | -81.6 | 210.0 | ECCC |
| co2_mnm_surface-insitu_19Representative | 24.3 | 154.0 | 8.0 | JMA |
| co2_ryo_surface-insitu_19Representative | 39.0 | 141.8 | 260.0 | JMA |
| co2_yon_surface-insitu_19Representative | 24.5 | 123.0 | 30.0 | JMA |

Table S2. The prior and predicted CO₂ fluxes (in PgC yr⁻¹) for 15 land and 11 ocean regions for 2001 - 2020. The predicted fluxes are shown for ensemble mean of “gc3t”, “gvjf” and all cases (“ensm”). The gc3t are based on the CASA fluxes for land and Takahashi fluxes for ocean. The gvjf prior is based on VISIT+GFED fluxes for land and JMA fluxes for ocean. The “ensm” is the ensemble mean of both gc3t and gvjf cases. The spread denotes the 1-sigma deviation from the mean CO₂ flux of 8-8 ensemble inversion cases for gc3t and gvjf as well as 16 ensemble inversion cases for “ensm”.

| Land Regions | Prior (gc3t/gvjf) | Predicted gc3t, gvjf, ensm (mean ± spread) | Ocean Regions | Prior (gc3t/gvjf) | Predicted gc3t, gvjf, ensm (mean ± spread) |
|----------------------|----------------------|---|----------------------|----------------------|---|
| Boreal N. America | 0.0/-0.49 | -0.34 ±0.07 -0.42±0.11 -0.38±0.10 | Northern Ocean | -0.28 / -0.28 | -0.27±0.03 -0.01±0.10 -0.14±0.15 |
| Temp. N. America | 0.0/-0.33 | -0.60±0.11 -0.59±0.16 -0.59±0.14 | North Pacific | -0.51/-0.60 | -0.59±0.01 -0.51±0.04 -0.55±0.05 |
| Brazil | 0.0/-0.17 | 0.04±0.08 -0.01±0.04 0.02±0.07 | South Pacific | -0.31/-0.54 | -0.3±0.01 -0.48±0.01 -0.39±0.09 |
| Central America | 0.0/-0.33 | -0.04±0.06 -0.24±0.03 -0.14±0.11 | East Pacific | 0.41 / 0.42 | 0.48±0.04 0.46±0.02 0.47±0.03 |
| Temp. S. America | 0.0/-0.36 | 0.04±0.06 -0.23±0.07 -0.10±0.15 | West Pacific | 0.06 / 0.06 | 0.06±0.0 0.07±0.01 0.07±0.01 |
| Northern Africa | 0.0/0.03 | -0.11±0.02 -0.0±0.05 -0.06±0.07 | North Atlantic | -0.21 / -0.27 | -0.28±0.02 -0.27±0.01 -0.27±0.02 |
| Central Africa | 0.0/0.12 | -0.18±0.07 0.1±0.05 -0.04±0.15 | Tropical Atlantic | 0.11 / 0.08 | 0.12±0.01 0.09±0.0 0.11±0.02 |
| Southern Africa | 0.0/0.15 | -0.08±0.01 0.17±0.01 0.05±0.12 | South Atlantic | -0.15 / -0.33 | -0.17±0.01 -0.31±0.01 -0.24±0.07 |
| Europe | 0.0/-0.54 | 0.08±0.07 -0.09±0.08 | Tropical Indian | 0.12 / 0.12 | 0.07±0.02 0.1±0.02 |

| | | | | | |
|----------------|-----------|---|---------------------|---------------|---|
| | | -0.0±0.11 | | | 0.09±0.03 |
| Russia | 0.0/-0.76 | -0.37±0.03 -0.33±0.05 -0.35±0.05 | South Indian | -0.43 / 0.53 | -0.43±0.01 -0.49±0.02 -0.46±0.03 |
| West Asia | 0.0/-0.11 | -0.04±0.04 -0.09±0.01 -0.06±0.04 | Southern Ocean | -0.23 / -0.24 | -0.29±0.02 -0.18±0.02 -0.23±0.06 |
| South Asia | 0.0/-0.23 | -0.10±0.10 -0.26±0.04 -0.18±0.11 | Global Total | | |
| East Asia | 0.0/-0.55 | -0.42±0.05 -0.57±0.04 -0.49±0.09 | Land | 0/-3.93 | -2.42±0.10 -2.73±0.20 -2.58±0.22 |
| Southeast Asia | 0.0/-0.17 | -0.25±0.08 0.0±0.05 -0.13±0.15 | Ocean | -1.4/-2.11 | -1.58±0.04 -1.51±0.07 -1.54±0.13 |
| Oceania | 0.0/-0.2 | -0.06±0.07 -0.17±0.03 -0.12±0.08 | Land+Ocean | -1.4/-6.06 | -4.01±0.08 -4.26±0.07 -4.14±0.14 |

Table S3: Correlation coefficient (r) and p values between the mean CO₂ flux (predicted/prior) anomaly and Multivariate ENSO Index (MEI) for 2001-2020 (columns 2-4). Correlation coefficients and p values for the prior and predicted mean seasonal cycles are given in the two columns on the right. Correlations in bold indicate statistically significant at 95% confidence intervals

| Regions | r for interannual variability | | | r for seasonal cycle | |
|---------------------|-------------------------------|-------------------------------|----------------------|----------------------|------------------------|
| | gc3t (predicted) | gvjf (predicted) | gvjf (prior) | prior gc3t-gvjf | predicted gc3t-gvjf |
| Land Regions | | | | | |
| Boreal N. America | -0.05 (0.44) | 0.07 (0.27) | 0.1 (0.13) | 0.77 (0.004) | 0.9 (0.001) |
| Temp. N. America | -0.07 (0.29) | -0.26 (0.002) | -0.2 (0.001) | 0.8 (0.002) | 0.97 (0.001) |
| Brazil | 0.44 (0.001) | 0.22 (0.001) | 0.28 (0.001) | 0.23 (0.48) | 0.63 (0.03) |
| Tropical America | 0.32 (0.001) | 0.47 (0.001) | 0.48 (0.001) | 0.39 (0.204) | 0.94 (0.001) |
| Temp. S. America | 0.54 (0.001) | 0.08 (0.19) | -0.04 (0.55) | 0.88 (0.001) | 0.74 (0.01) |
| Europe | 0.19 (0.003) | 0.23 (0.001) | 0.09 (0.17) | 0.83 (0.001) | 0.92 (0.001) |
| Northern Africa | 0.46 (0.001) | 0.26 (0.001) | 0.15 (0.02) | 0.91 (0.001) | 0.88 (0.001) |
| Central Africa | 0.51 (0.001) | 0.39 (0.001) | 0.29 (0.001) | -0.19 (0.55) | 0.04 (0.9) |
| Southern Africa | 0.26 (0.001) | 0.26 (0.001) | 0.23 (0.000 1) | 0.90 (0.001) | 0.95 (0.001) |
| Russia | -0.01 (0.87) | -0.11 (0.08) | -0.08 (0.19) | 0.79 (0.002) | 0.92 (0.001) |
| West Asia | 0.19 (0.003) | 0.16 (0.01) | 0.06 (0.35) | 0.83 (0.001) | 0.91 (0.001) |
| South Asia | 0.2 (0.002) | 0.1 (0.14) | 0.09 (0.18) | 0.28 (0.38) | 0.23 (0.47) |

| | | | | | |
|----------------------|-------------------------------|--------------------------------|-------------------------------|------------------|-----------------|
| East Asia | 0.03 (0.67) | -0.17 (0.008) | -0.21 (0.001) | 0.28 (0.38) | 0.83 (0.001) |
| Southeast Asia | 0.29 (0.001) | 0.61 (0.001) | 0.62 (0.000) | 0.19 (0.56) | 0.15 (0.65) |
| Oceania | 0.17 (0.01) | 0.54 (0.001) | 0.56 (0.001) | -0.48 (0.12) | -0.36 (0.25) |
| Global total | 0.43 (0.001) | 0.51 (0.001) | 0.46 (0.001) | 0.80 (0.002) | 0.98 (0.001) |
| Ocean regions | | | | | |
| Northern Ocean | 0.09 (0.17) | 0.28 (0.001) | 0.16 (0.01) | -0.16 (0.62) | 0.46 (0.13) |
| North Pacific | 0.1 (0.11) | 0.02 (0.72) | -0.13 (0.05) | 0.99 (0.001) | 0.69 (0.01) |
| East Pacific | 0.1 (0.15) | -0.35 (0.001) | -0.49 (0.001) | 0.69 (0.013) | 0.83 (0.001) |
| West Pacific | 0.09 (0.13) | -0.62 (0.001) | -0.7 (0.001) | -0.33 (0.29) | 0.69 (0.01) |
| South Pacific | -0.1 (0.13) | -0.24 (0.0002) | -0.11 (0.08) | 0.97 (0.001) | 0.98 (0.001) |
| North Atlantic | -0.19 (0.002) | -0.14 (0.028) | -0.17 (0.008) | 0.99 (0.001) | 0.92 (0.001) |
| Tropical Atlantic | 0.39 (0.001) | 0.38 (0.001) | 0.1 (0.11) | -0.10 (0.76) | 0.63 (0.03) |
| South Atlantic | 0.0 (0.97) | 0.04 (0.56) | 0.01 (0.83) | 0.52 (0.08) | 0.65 (0.02) |
| Tropical Indian | 0.36 (0.001) | 0.09 (0.17) | 0.05 (0.46) | 0.93 (0.001)) | 0.78 (0.001) |
| South Indian | 0.32 (0.001) | 0.25 (0.001) | 0.07 (0.25) | 0.94 (0.001) | 0.95 (0.001) |
| Southern Ocean | 0.23 (0.0004) | 0.11 (0.10) | -0.08 (0.20) | 0.89 (0.001) | 0.91 (0.001) |
| Global total | 0.3 (0.001) | -0.07 (0.2) | -0.24 (0.001) | 0.95 (0.001) | 0.58 (0.05) |

Table S4. Mean model-observation bias at different atmospheric layers for individual aircraft observations sites for their available period. Biases greater than ± 2 ppm are marked in red, and those greater than ± 1 ppm are marked in blue. Model simulation only for ensm fluxes are used.

| Site name | LT (0 - 2 Km) | | MT (3-5 Km) | | UT (6-8 Km) | | All (0 - 8 Km) | |
|---|-----------------|------------------|-----------------|------------------|-----------------|------------------|-----------------|------------------|
| | Mean Bias (ppm) | # of data points | Mean Bias (ppm) | # of data points | Mean Bias (ppm) | # of data points | Mean Bias (ppm) | # of data points |
| co2_aao_aircraft-pfp_1_allvalid | 0.11 | 1442 | 0.48 | 784 | nan | 0 | 0.28 | 2810 |
| co2_above_aircraft-raft-insitu_1_allvalid | 0.1 | 44443 | 1.31 | 27232 | nan | 0 | 0.77 | 95415 |
| co2_above_aircraft-pfp_1_allvalid | -0.16 | 193 | 1.92 | 74 | nan | 0 | 0.75 | 344 |
| co2_acg_aircraft-t-insitu_1_allvalid | -0.87 | 4251 | 1.32 | 1683 | 2.23 | 4310 | 0.9 | 14313 |
| co2_acg_aircraft-pfp_1_allvalid | -0.22 | 675 | 1.03 | 264 | 0.91 | 296 | 0.43 | 1520 |
| co2_act_aircraft-insitu_428_allvalid-b200 | -0.47 | 198597 | 0.34 | 81425 | -0.57 | 17218 | -0.17 | 347177 |
| co2_act_aircraft-insitu_428_allvalid-c130 | -0.1 | 122769 | 0.34 | 87700 | -0.09 | 40766 | 0.06 | 347919 |
| co2_act_aircraft-pfp_1_allvalid-b200 | -0.95 | 1987 | 0.39 | 563 | -0.3 | 123 | -0.49 | 3022 |
| co2_act_aircraft-pfp_1_allvalid-c130 | -0.14 | 1451 | 0.58 | 614 | -0.04 | 240 | 0.1 | 2897 |
| co2_aia_aircraft-flask_2_represe | -0.14 | 160 | 0.01 | 82 | 0.1 | 51 | -0.05 | 353 |

| ntative | | | | | | | | |
|---|--------------|-------|--------------|-------|-------------|-------|-------------|--------|
| co2_alf_aircraft - pfp_26_represe ntative | -0.06 | 333 | 0.01 | 245 | nan | 0 | -0.09 | 684 |
| co2_aoa_aircraf t- flask_19_allvali d | -0.04 | 206 | -0.18 | 237 | -0.03 | 1161 | -0.04 | 2500 |
| co2_arcpac2008 _aircraft- insitu_114_allv alid | 0.01 | 7489 | -1.13 | 6146 | -0.49 | 3493 | -0.66 | 22586 |
| co2_arctas_irc raft- insitu_428_allv alid-dc8 | -1.25 | 17529 | 0.07 | 10376 | 0.42 | 9382 | -0.38 | 46730 |
| co2_bgi_aircraf t-pfp_1_allvalid | -0.99 | 71 | 0.23 | 93 | -0.08 | 89 | -0.13 | 334 |
| co2_bne_aircraf t-pfp_1_allvalid | -0.46 | 259 | -0.08 | 248 | -0.45 | 218 | -0.28 | 972 |
| co2_brz_aircraf t- insitu_20_allval id | -0.31 | 77277 | 1.82 | 2778 | nan | 0 | 0.11 | 100259 |
| co2_calnex2010 _aircraft- insitu_114_allv alid | -3.66 | 29604 | -0.19 | 4234 | 0 | 40 | -2.7 | 39366 |
| co2_car_aircraft -pfp_1_allvalid | -1.33 | 138 | 0 | 2548 | -0.01 | 1964 | -0.07 | 6698 |
| co2_cma_aircra ft- pfp_1_allvalid | -1.09 | 803 | 0.41 | 541 | -0.11 | 546 | -0.28 | 2610 |
| co2_cob2003b_ aircraft- insitu_59_allval id | 0.45 | 5228 | 0.95 | 3973 | 0.38 | 4122 | 0.66 | 16692 |
| co2_cob2004_a | -0.6 | 18052 | 1.21 | 10328 | 1.75 | 11583 | 0.82 | 50688 |

| ircraft-insitu_59_allval_id | | | | | | | | |
|--|-------|--------|-------|--------|-------|--------|-------|---------|
| co2_cob_aircraft-flask_1_allvalid | -0.78 | 61 | -1.03 | 18 | -0.56 | 1 | -0.54 | 108 |
| co2_cob_aircraft-insitu_59_allval_id | 2.53 | 17434 | 1.09 | 16319 | 0.95 | 8037 | 1.52 | 55783 |
| co2_cob_aircraft-pfp_1_allvalid | 1.39 | 68 | 0.27 | 73 | 0.69 | 30 | 0.7 | 227 |
| co2_con_aircraft-flask_42_allvalid | -0.22 | 9 | -0.34 | 14 | -0.32 | 26 | -0.31 | 65 |
| co2_con_aircraft-insitu_42_allval_id | -1.23 | 504283 | -0.39 | 670363 | -0.25 | 631220 | -0.55 | 2449936 |
| co2_crv_aircraft-pfp_1_allvalid | -2.59 | 1601 | 0.95 | 107 | nan | 0 | -1.68 | 2103 |
| co2_dc3_aircraft-insitu_428_allvalid-dc8 | 0.6 | 6800 | -0.72 | 5511 | -1.21 | 3656 | -0.36 | 21178 |
| co2_dc3_aircraft-insitu_428_allvalid-falcon | 1.64 | 1066 | -2.33 | 3711 | -2.13 | 4074 | -1.7 | 12459 |
| co2_discover-aq_aircraft-insitu_428_allvalid-c130-co | -9.47 | 5968 | -0.44 | 8304 | -1.19 | 301 | -3.57 | 21114 |
| co2_discover-aq_aircraft-insitu_428_allvalid-p3b-ca | -5.82 | 18973 | -0.46 | 640 | nan | 0 | -4.2 | 26822 |
| co2_discover-aq_aircraft- | -7.43 | 8194 | -0.81 | 8840 | -0.55 | 49 | -3.5 | 30057 |

| | | | | | | | | |
|---|-------|-------|-------|-------|-------|-------|-------|-------|
| insitu_428_allv alid-p3b-co | | | | | | | | |
| co2_discover- aq_aircraft- insitu_428_allv alid-p3b-tx | -4.42 | 14239 | 0.43 | 6416 | 0.5 | 932 | -2.36 | 25077 |
| co2_dnd_aircraf t-pfp_1_allvalid | -0.49 | 547 | 0.18 | 487 | 0.12 | 438 | -0.02 | 2075 |
| co2_eco_aircraf t- insitu_1_allvali d | -2.19 | 26197 | -0.31 | 1463 | nan | 0 | -1.95 | 30468 |
| co2_esp_aircraf t-pfp_1_allvalid | -0.4 | 1772 | 0.37 | 1494 | nan | 0 | 0.08 | 4563 |
| co2_etl_aircraft -pfp_1_allvalid | -0.47 | 1082 | 0.56 | 638 | 0.59 | 276 | 0.12 | 3184 |
| co2_ftl_aircraft- pfp_1_allvalid | -0.18 | 12 | 0.39 | 51 | nan | 0 | 0.17 | 90 |
| co2_fwi_aircraf t-pfp_1_allvalid | -0.39 | 79 | 0.29 | 102 | 0.15 | 95 | 0.17 | 361 |
| co2_gsfc_aircra ft- insitu_430_allv alid | 0.38 | 5903 | 0.8 | 11968 | 0.81 | 16066 | 0.77 | 43427 |
| co2_haa_aircraf t-pfp_1_allvalid | 0.03 | 260 | -0.13 | 543 | 0.04 | 370 | -0.07 | 1627 |
| co2_hfm_aircra ft- pfp_1_allvalid | -1.08 | 451 | 0.37 | 392 | 0.15 | 361 | -0.14 | 1630 |
| co2_hil_aircraft -pfp_1_allvalid | -0.48 | 593 | -0.2 | 727 | -0.36 | 672 | -0.31 | 2622 |
| co2_hip_aircraf t- insitu_59_allval id | -0.14 | 21818 | 0.42 | 19025 | 0.31 | 18172 | 0.21 | 77048 |
| co2_iagos- caribic_aircraft- flask_457_allva | 1.97 | 2 | -0.19 | 29 | -0.16 | 29 | -0.11 | 74 |

| lid | | | | | | | | |
|--|-------|-------|-------|------|-------|------|-------|-------|
| co2_iagos-caribic_aircraft-insitu_457_allvalid | -1.18 | 993 | 0.58 | 1768 | 0.65 | 6053 | 0.45 | 11322 |
| co2_intex-b_aircraft-insitu_428_allvalid-dc8 | -0.45 | 1692 | -0.27 | 1327 | -0.48 | 1118 | -0.37 | 5447 |
| co2_intex-na_aircraft-insitu_428_allvalid-dc8 | 2.56 | 14469 | 1.61 | 7889 | 1.55 | 7626 | 2.08 | 36495 |
| co2_inx_aircraft-pfp_1_allvalid | -2.56 | 238 | 0.11 | 12 | nan | 0 | -2.23 | 273 |
| co2_korus-aq_aircraft-insitu_428_allvalid-dc8 | -3.84 | 34197 | -0.08 | 5307 | -0.56 | 9006 | -2.49 | 55612 |
| co2_lef_aircraft-pfp_1_allvalid | -0.29 | 1884 | 0.25 | 1115 | nan | 0 | -0.03 | 3976 |
| co2_mci_aircraft-pfp_1_allvalid | -1.29 | 65 | -0.5 | 10 | nan | 0 | -1.14 | 92 |
| co2_mrc_aircraft-pfp_1_allvalid | 0.15 | 58 | -0.32 | 1 | nan | 0 | 0.13 | 65 |
| co2_nha_aircraft-pfp_1_allvalid | -0.9 | 1373 | 0.45 | 789 | 0.06 | 536 | -0.21 | 3633 |
| co2_oil_aircraft-pfp_1_allvalid | -0.05 | 87 | 0.51 | 113 | 0.11 | 106 | 0.31 | 399 |
| co2_orc_aircraft-insitu_3_allvalidd-merge10 | -0.14 | 8027 | -0.16 | 3635 | -0.04 | 3911 | -0.12 | 19414 |
| co2_pfa_aircraft-pfp_1_allvalid | 0.08 | 1152 | 0.41 | 1327 | 0.51 | 781 | 0.28 | 4522 |
| co2_rba-b_aircraft- | -0.66 | 334 | -0.47 | 231 | nan | 0 | -0.65 | 674 |

| | | | | | | | | |
|--|-------|-------|-------|------|-------|------|-------|-------|
| pfp_26_representative | | | | | | | | |
| co2_rta_aircraft-pfp_1_allvalid | 0.18 | 437 | 0.03 | 792 | 0.12 | 332 | 0.06 | 2235 |
| co2_sam_aircraft-pfp_1_allvalid | -0.68 | 35 | -1.31 | 29 | -0.59 | 23 | -1.08 | 118 |
| co2_san_aircraft-pfp_1_allvalid | 0.3 | 11 | -0.26 | 90 | nan | 0 | -0.3 | 154 |
| co2_san_aircraft-pfp_26_representative | -0.82 | 1309 | -0.31 | 719 | nan | 0 | -0.66 | 2458 |
| co2_sca_aircraft-pfp_1_allvalid | -0.84 | 525 | -0.02 | 811 | -0.32 | 746 | -0.24 | 2892 |
| co2_seac4rs_aircraft-insitu_428_allvalid-ER2 | 0.82 | 4 | 1.1 | 233 | 0.54 | 210 | 0.81 | 590 |
| co2_seac4rs_aircraft-insitu_428_allvalid-dc8 | 1.03 | 18802 | 0.09 | 6688 | 0.69 | 6991 | 0.75 | 39914 |
| co2_senex2013_aircraft-insitu_114_allvalid | 0.9 | 30012 | 1.04 | 4440 | 1.1 | 467 | 0.88 | 39610 |
| co2_sgp_aircraft-pfp_1_allvalid | -0.22 | 2374 | -0.25 | 1623 | 1.08 | 9 | -0.23 | 5513 |
| co2_songnex2015_aircraft-insitu_114_allvalid | 0.04 | 20404 | -0.11 | 5418 | -0.78 | 4398 | -0.1 | 42549 |
| co2_start08_aircraft-insitu_59_allvalid | -0.85 | 1421 | -0.46 | 2548 | -0.54 | 1985 | -0.57 | 8107 |
| co2_tab_aircraft- | -1.98 | 228 | -0.48 | 163 | nan | 0 | -1.33 | 463 |

| | | | | | | | | |
|--|-------|-------|-------|-------|-------|-------|-------|-------|
| pfp_26_represe ntative | | | | | | | | |
| co2_texaqs2006 _aircraft- insitu_114_allv alid | -4.48 | 28586 | 0.5 | 2046 | nan | 0 | -3.87 | 32653 |
| co2_tgc_aircraft -pfp_1_allvalid | -0.65 | 382 | -0.34 | 694 | -0.36 | 594 | -0.37 | 2337 |
| co2_thd_aircraf t-pfp_1_allvalid | -1.06 | 598 | 0.32 | 589 | -0.05 | 535 | -0.15 | 2329 |
| co2_tom_aircra ft- insitu_1_allvali d | 0.02 | 25586 | 0.13 | 15139 | 0.17 | 17915 | 0.1 | 74184 |
| co2_trace- p_aircraft- insitu_428_allv alid-dc8 | -0.07 | 11133 | -0.18 | 7003 | -0.34 | 6097 | -0.2 | 30887 |
| co2_trace- p_aircraft- insitu_428_allv alid-p3b | 0.32 | 16956 | -0.15 | 13902 | 0.1 | 6935 | 0.04 | 50121 |
| co2.ulb_aircraf t-pfp_1_allvalid | 0.36 | 169 | 0.17 | 223 | nan | 0 | 0.28 | 546 |
| co2.wbi_aircraf t-pfp_1_allvalid | -0.4 | 532 | 0.01 | 653 | -0.36 | 617 | -0.22 | 2366 |

Testing the effect of annually repeating G matrix vs interannually varying G matrix:

This quasi-IAV meteorology approach was done first in Patra et al. (2016) followed by Chandra et al. (2021).

In our inversion, monthly-mean regional a posteriori fluxes (\vec{s}) are based on the observation data (\vec{d}_{obs}) and model simulation (\vec{d}_{ACTM}) of a priori fluxes (\vec{s}_0) (Eq. 2). This equation shows that the a priori model simulation d_{ACTM} is the most important term for the correction (increase or decrease) of the a priori fluxes. Green's function determines the magnitude of flux corrections. Noting the importance of the ($d_{obs} - d_{ACTM}$) term compared to J , while the latter is 84 (inversion region) \times 12 (months per year) \times 4 years (pulse duration) times more computationally expensive, we have decided to put more focus on \vec{d}_{ACTM} , e.g., testing various emission combinations, transport sensitivity in this study. The figure below shows an example of the “CO₂” inversion cases using interannually varying (IAV) meteorology (IAV for both \vec{d}_{ACTM} and J -matrix) and quasi-IAV meteorology (IAV for both \vec{d}_{ACTM} but repeating 2009 J -matrix). This plot clearly shows that the flux anomalies can be consistently estimated by the inverse modelling by our quasi-IAV approach. This success is achieved because the forward simulation of prior fluxes contains most of the spatial and temporal variations, and the correction fluxes by inversions are only incremental to the priors for most regions (Fig. 8, Fig. S1).

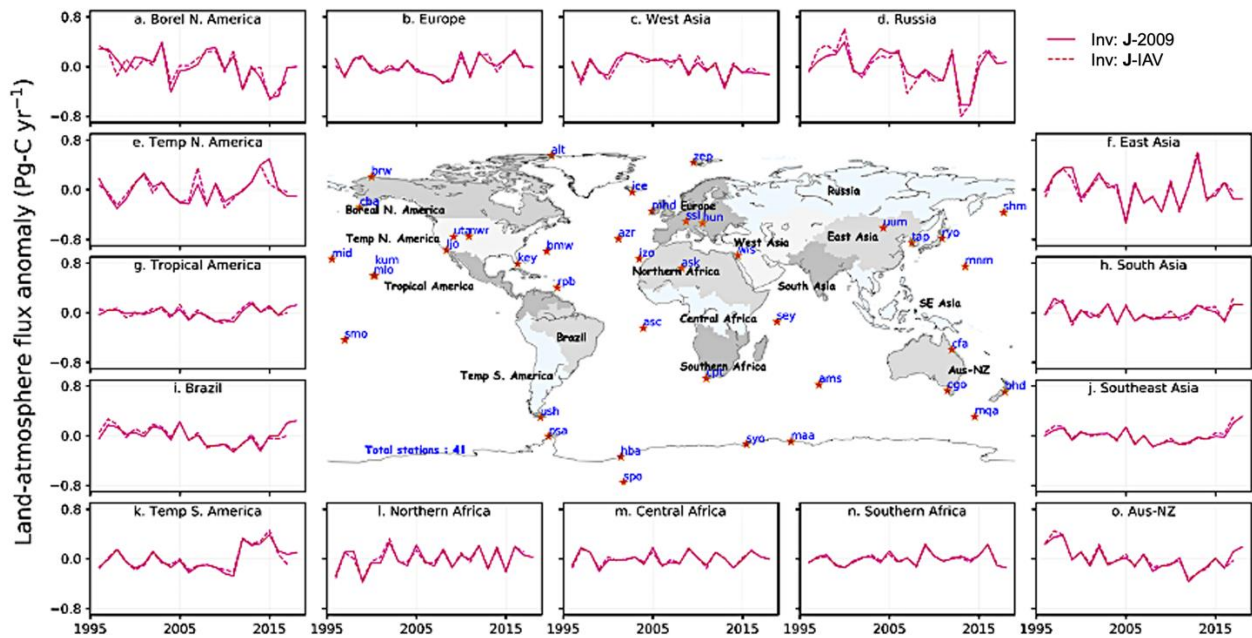


Figure S1: Regional CO₂ fluxes anomalies, similar to Fig. 6, for showing the effect of inter-annually varying J -matrix (J-IAV) vs annually repeating J -matrix corresponding to the year 2009 (J-2009). This checking was conducted using the inversion results submitted to GCP-2018 budget (Le Quéré et al., 2018). Please note that the PFU, MDU and other model setups were differently set at that time and the flux results cannot be compared with those in the present study.

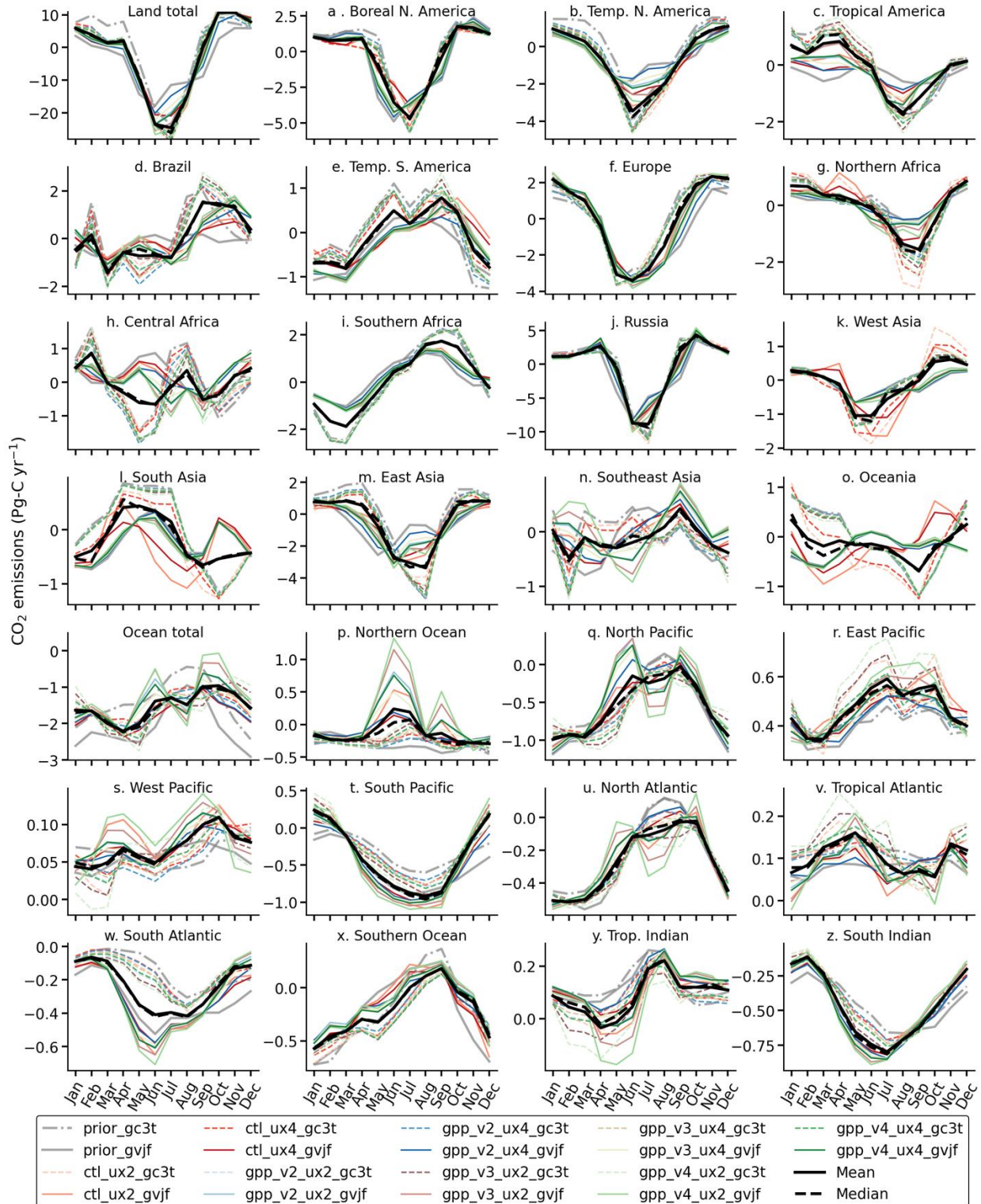


Figure S2. Seasonal variations in monthly-mean CO₂ fluxes at regional scales over 15 land (upper 4 rows) and 11 ocean (lower 3 rows) regions, along with global land and ocean totals. Note that all panels use different y-scale. The seasonal cycles only over a few (ill-constrained) regions are significantly corrected by inversions.

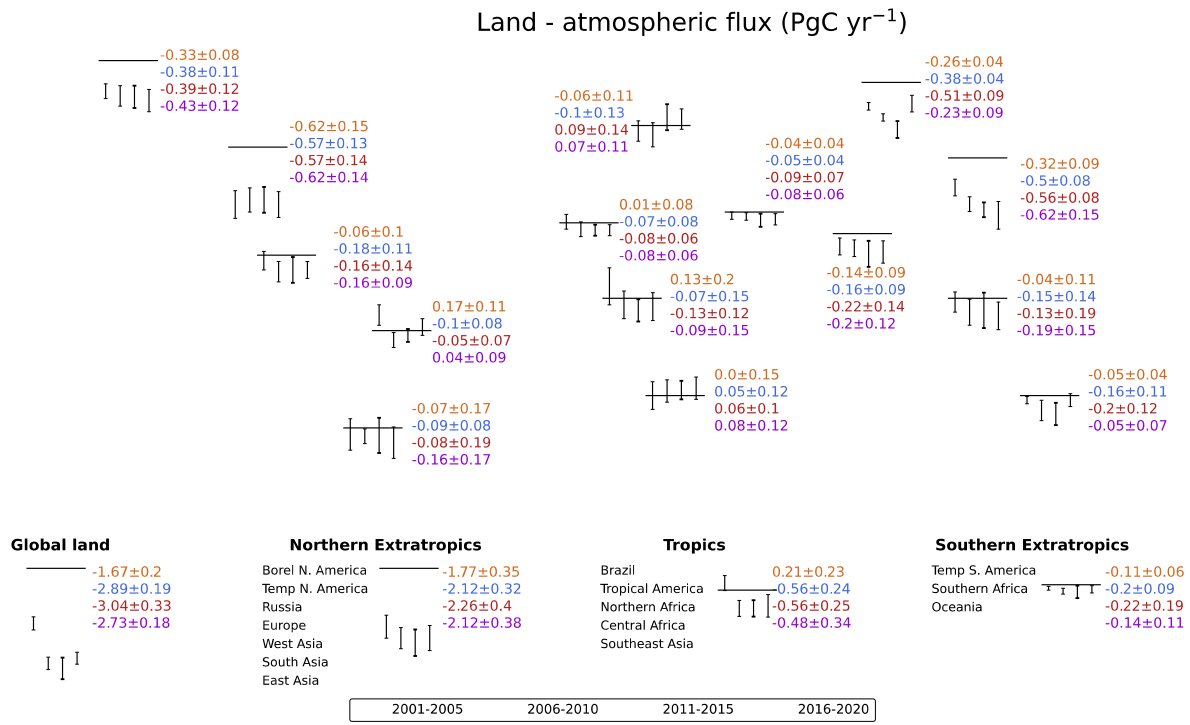


Fig S3. Mean CO_2 fluxes and spread ($\pm 1\sigma$) among 16 inversion cases over global, three aggregated latitudinal bands and 15 aggregated land regions. The bars in the down-facing directions represent carbon sinks, whereas the bars in the upward-facing directions represent carbon source.

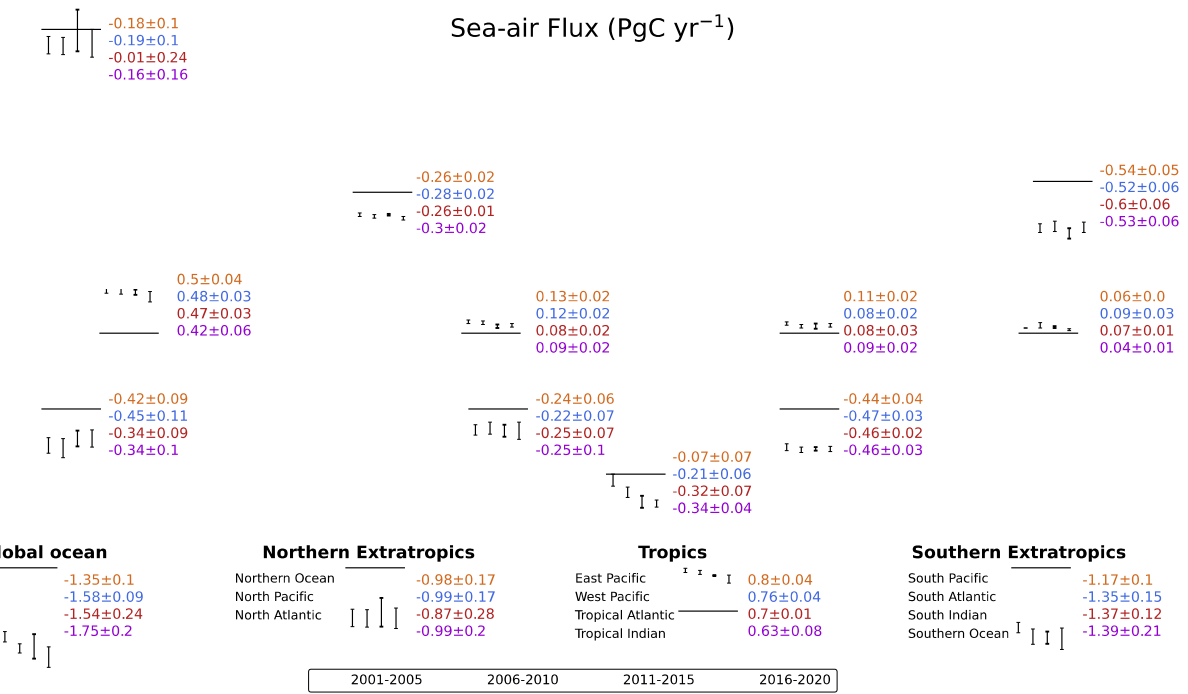


Fig S4. Mean CO_2 fluxes and spread among 16 inversion cases ($\pm 1\sigma$) over global, three aggregated latitudinal bands and 11 aggregated ocean regions. The bars in the down-facing directions represent carbon sinks, whereas the bars in the upward-facing directions represent carbon source.

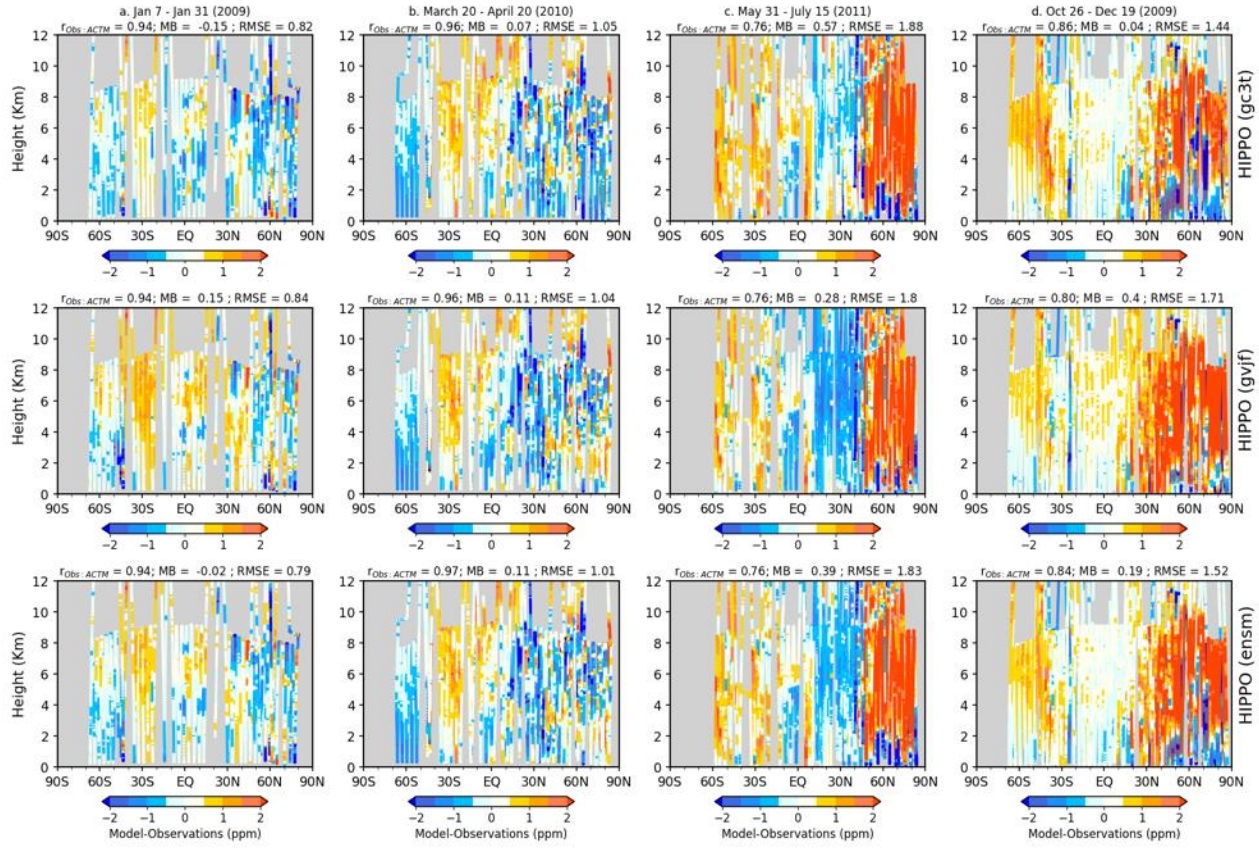


Figure S5: Mismatch between simulated and measured CO₂ during HIPPO aircraft campaigns. The observed and modelled data are binned and averaged at intervals of 2.5° latitude and 500-meter altitude. The grey area shows no flights at those altitudes and altitudes. Modelled mole fractions were simulated from the three posterior flux cases. The upper, middle, and the bottom row show simulations for “gc3t”, “gvjf”, and “ensm” cases, respectively. The correlation coefficients (r), mean bias (MB), and root-mean-square error between observations and simulations are also shown in the title.

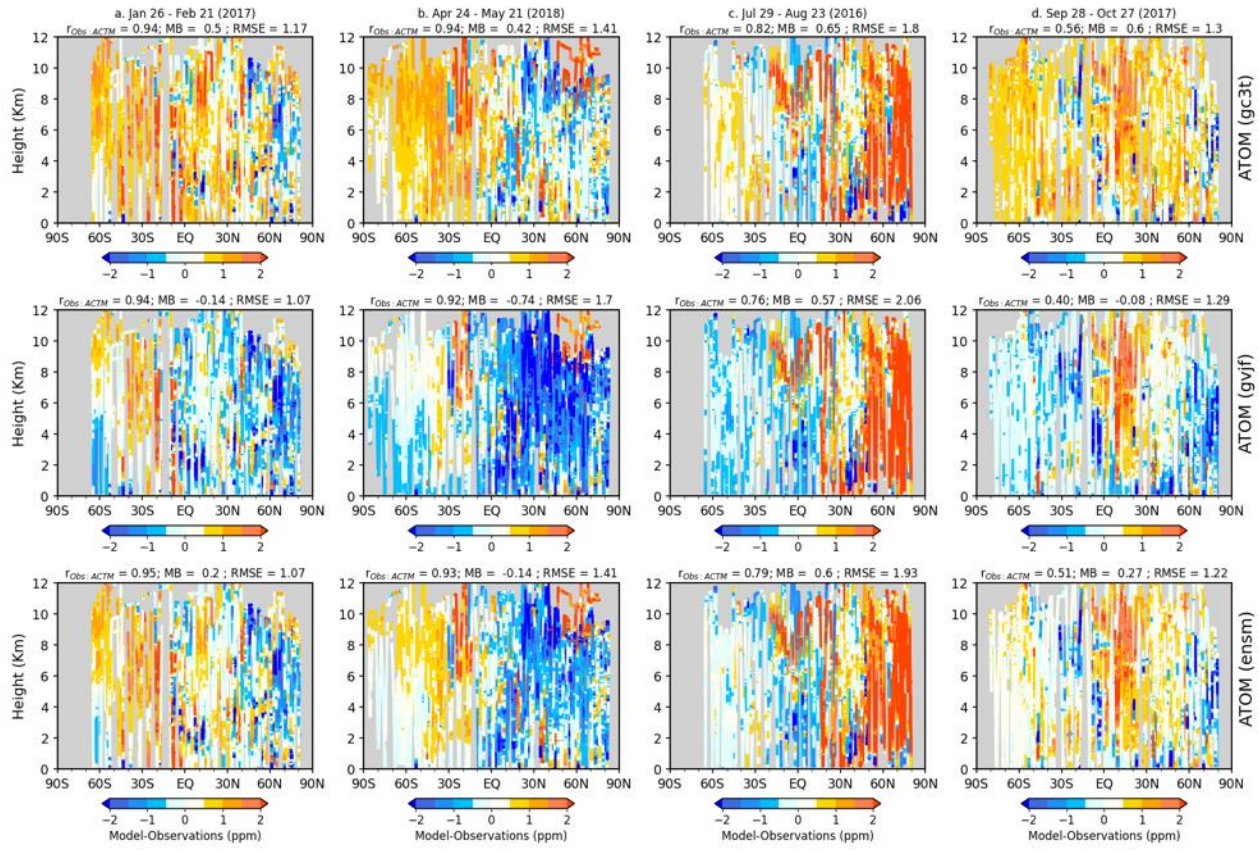


Figure S6: Same as S2, but for ATom aircraft campaigns.

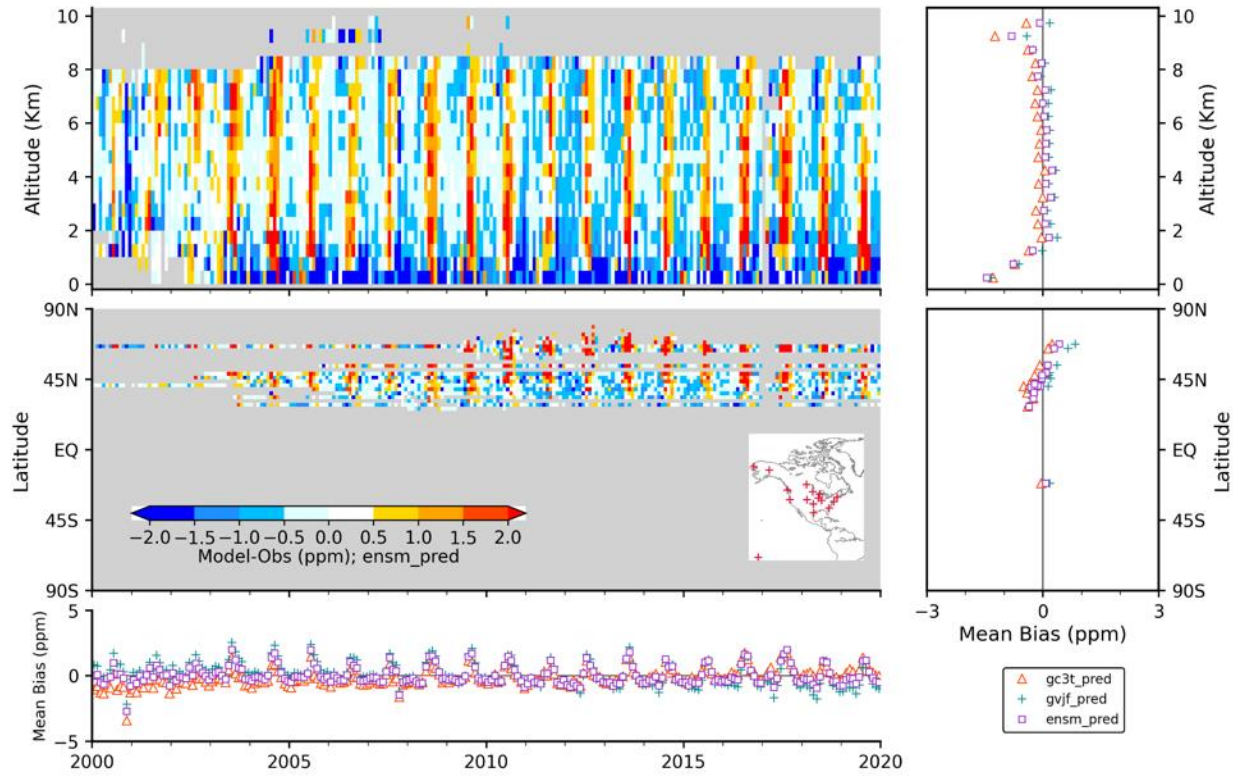


Figure S7. Validation of simulated CO₂ mixing ratios using regular NOAA aircraft profiles over 16 sites (see the location in the middle panel's inset map). The top panel shows bias (model minus observations) as a function of altitude, and the middle shows the mean bias in the free troposphere (defined between 2 and 8 Km) as a function of latitude. The bottom panel shows the monthly mean bias in the free troposphere over all the latitudes. The contour plots are shown for the “ensm” prescribed flux case, while other plots are shown for all three prescribed emission cases.

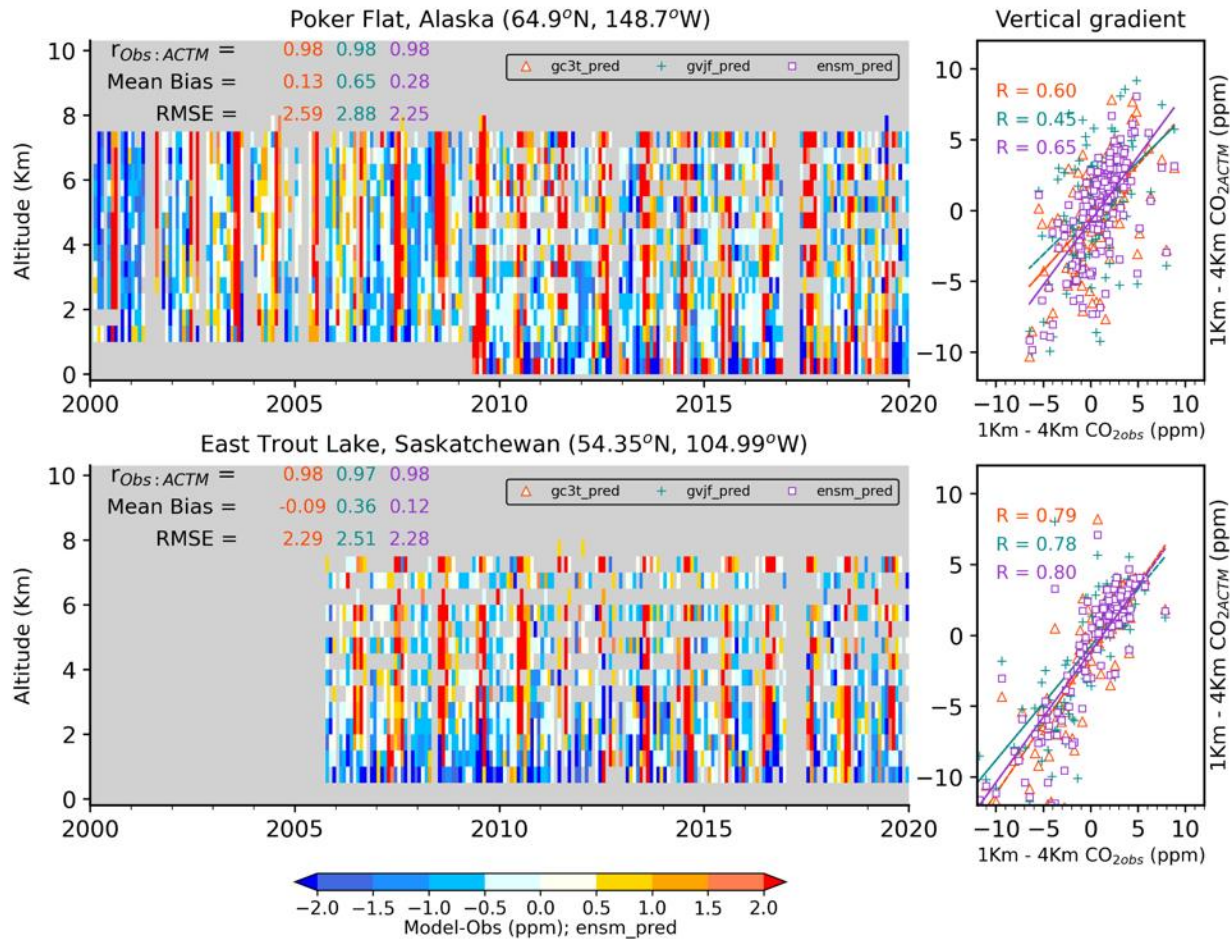


Figure S8. Validation of simulated CO_2 mixing ratios using regular NOAA aircraft profiles over two sites located in boreal North America (see also Figure xx for the location of profiles). The left panel shows the bias (model minus observations) as a function of altitude, and the right panel shows the scatter plot between the observed and modelled vertical gradient using three prescribed emissions.

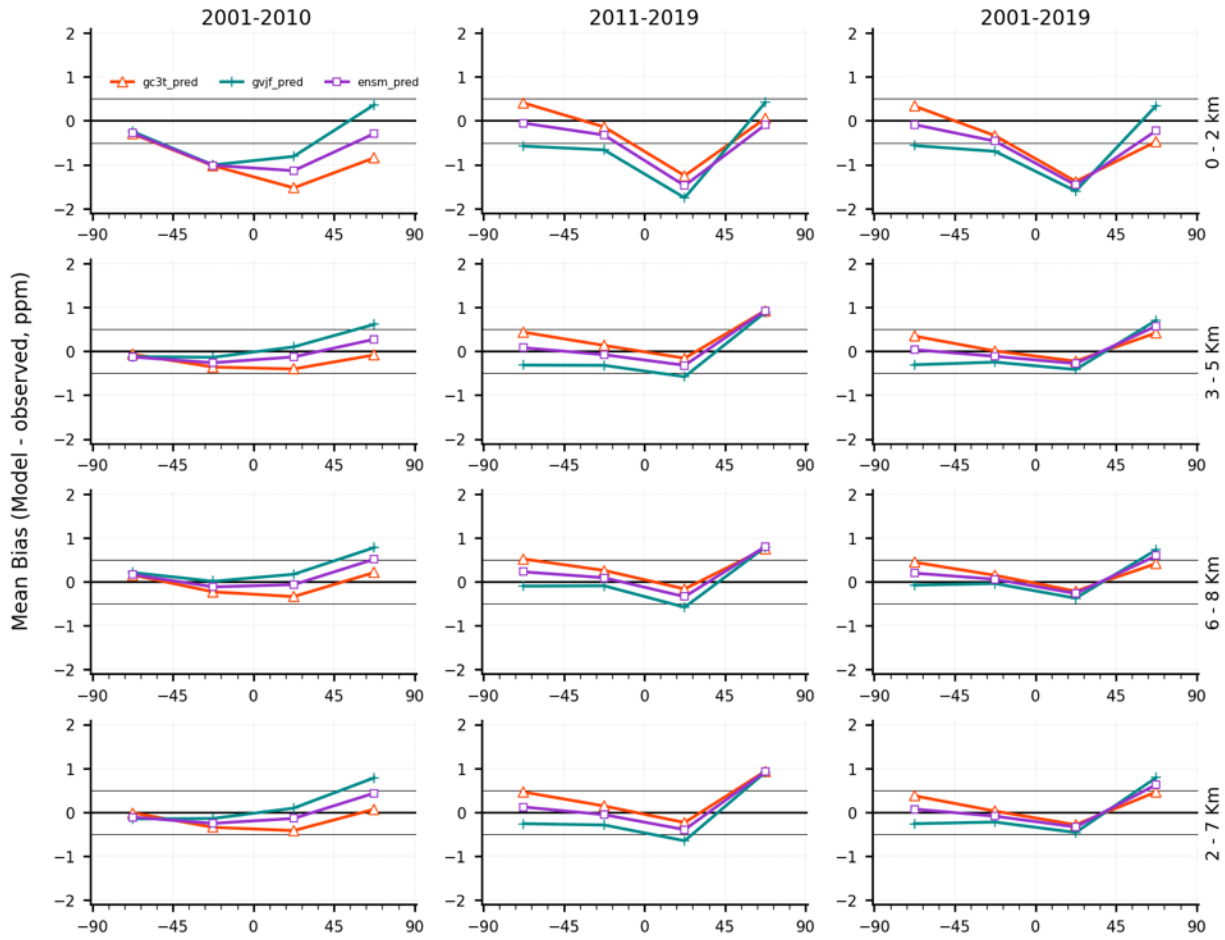


Figure S9. Evaluation of the atmospheric inversion products. The mean of the model minus observations is shown for four latitude bands at four altitude ranges in three periods: (a) 2001–2010, (b) 2011–2020, (c) 2001–2020. The simulations from three inversion cases are compared to independent CO₂ measurements made onboard aircraft over many places of the world between 2 and 8 km above sea level. Aircraft measurements archived in the Cooperative Global Atmospheric Data Integration Project (CGADIP, 2020) from sites, campaigns, or programs that cover at least 9 months between 2001 and 2020, and that have not been assimilated have been used to compute the biases of the differences in four 45° latitude bins. Land and ocean data are used without distinction.

References:

Chandra, N., Patra, P. K., Bisht, J. S. H., Ito, A., Umezawa, T., Saigusa, N., Morimoto, S., Aoki, S., JANSSENS-MAENHOUT, G., Fujita, R., Takigawa, M., Watanabe, S., SAITO, N. and Canadell, J. G.:

Emissions from the Oil and Gas Sectors, Coal Mining and Ruminant Farming Drive Methane Growth over the Past Three Decades, *J. Meteorol. Soc. Japan. Ser. II*, 99, doi:10.2151/jmsj.2021-015, 2021.

Le Quéré, C., Andrew, R. M., Friedlingstein, P., Sitch, S., Hauck, J., Pongratz, J., Pickers, P. A., Korsbakken, J. I., Peters, G. P., Canadell, J. G., Arneth, A., Arora, V. K., Barbero, L., Bastos, A., Bopp, L., Chevallier, F., Chini, L. P., Ciais, P., Doney, S. C., Gkritzalis, T., Goll, D. S., Harris, I., Haverd, V., Hoffman, F. M., Hoppema, M., Houghton, R. A., Hurt, G., Ilyina, T., Jain, A. K., Johannessen, T., Jones, C. D., Kato, E., Keeling, R. F., Goldewijk, K. K., Landschützer, P., Lefèvre, N., Lienert, S., Liu, Z., Lombardozzi, D., Metzl, N., Munro, D. R., Nabel, J. E. M. S., Nakaoka, S., Neill, C., Olsen, A., Ono, T., Patra, P., Peregon, A., Peters, W., Peylin, P., Pfeil, B., Pierrot, D., Poulter, B., Rehder, G., Resplandy, L., Robertson, E., Rocher, M., Rödenbeck, C., Schuster, U., Schwinger, J., Séférian, R., Skjelvan, I., Steinhoff, T., Sutton, A., Tans, P. P., Tian, H., Tilbrook, B., Tubiello, F. N., van der Laan-Luijkx, I. T., van der Werf, G. R., Viovy, N., Walker, A. P., Wiltshire, A. J., Wright, R., Zaehle, S. and Zheng, B.: Global Carbon Budget 2018, *Earth Syst. Sci. Data*, 10(4), 2141–2194, doi:10.5194/essd-10-2141-2018, 2018.

Patra, P. K., T. Saeki, E. J. Dlugokencky, K. Ishijima, T. Umezawa, A. Ito, S. Aoki, et al.: Regional Methane Emission Estimation Based on Observed Atmospheric Concentrations (2002-2012), *J. Meteorol. Soc. Japan. Ser. II*, 94, 91–113. <https://doi.org/10.2151/jmsj.2016-006>.